Ambiguities in strong absorptionlike S functions and in the corresponding potentials for heavy-ion collisions

C. Steward* and H. Fiedeldey†
Department of Physics, University of South Africa, P.O. Box 392, Pretoria, 0001 South Africa

K. Amos and L. J. Allen
School of Physics, University of Melbourne, Parkville, Victoria 3052, Australia
(Received 17 March 1994)

A semiclassical (WKB) method within fixed energy inverse scattering theory has been used to analyze the differential cross section from the elastic scattering of 1449 MeV ^{12}C ions off of ^{208}Pb and of 1503 MeV ^{16}O ions off of ^{12}C. Excellent, statistically significant, fits to the ^{12}C-^{208}Pb experimental data have been found using a McIntyre form for the scattering function but with diverse sets of parameter values. There are corresponding diverse interaction potentials. To fit the ^{16}O-^{12}C data, a Regge pole term was needed to supplement the McIntyre form. Inversion of those scattering functions resulted in interaction potentials that vary noticeably within the sensitive radial regions. In addition, conventional optical model potentials have been obtained with which direct solution of the Schrödinger equations result in similar excellent fits to the data. It is shown that these large ambiguities in the potentials are due, in the main, to the limited angular range of the cross-section data and although the corresponding cross-section shapes beyond the measured scattering angle range for the ^{12}C-^{208}Pb collision vary over many orders of magnitude, it is unlikely that experiments can be made sensitive enough to select from among them because those cross sections are so small.

PACS number(s): 24.10.−i, 25.70.Bc

I. INTRODUCTION

In recent years, fixed energy inverse scattering methods [1] have proven an interesting means of analyzing experimental elastic scattering data [2–5]. The aim of such methods is to determine an effective interaction acting between colliding nuclear ions starting from a set of S functions that have been obtained by fitting differential cross-section data. While fully quantal inversion calculations can be made [4,5], the semiclassical WKB inversion scheme [3] has been found to be both stable and accurate in defining smooth potentials to small radii. WKB inversion is the approach used herein, as the approximation limits are not breached for the reactions to be studied and the simplicity of the method commends it. Nevertheless, full quantal inversion was made in two cases to ensure that the WKB scheme was accurate. Results were found that essentially were identical to those from the WKB method.

In heavy-ion scattering, many partial waves are involved and if the scattering interaction is assumed to be a smooth function, then the S functions will be smooth functions of angular momentum. Whence in analyses of most cross-section data, strong absorption model (SAM) parametrizations of those S functions are very useful. Indeed, the known strong absorptive character of most heavy-ion collisions was exploited to define various (SAM) forms of the nuclear S functions [6] long before most attempts to analyze data with phenomenological, coordinate space, local optical model potentials. It has been found that, amongst the strong absorption models, the five-parameter McIntyre form [7] provides the best fits to elastic scattering data at a variety of energies [8] and particularly so for cases with Fresnel shape in the differential cross-section data (e.g., from scattering off of targets with mass in excess of ^{40}Ca). The 1449 MeV ^{12}C-^{208}Pb differential cross section [9] is typical of such data and hence its use in our investigations of ambiguities involved in obtaining local scattering potentials by inversion methods. The 1503 MeV ^{16}O-^{12}C data [10] reveals an oscillating structure in the cross section typical of Fraunhofer scattering. Such structure is not as reflective of strong absorption as the heavy target results but nevertheless it can be fit using the McIntyre form of an S function; albeit usually needing the addition of a Regge pole or two to get statistically significant fits. This data set is typical of most experimental sets from light-ion scattering off of light mass targets (i.e., with masses less than ^{40}Ca).

Whether data are investigated by direct or inverse methods of analysis, the process involves an intermediate step namely the specification of the S matrix, S_l, (or equivalently, the scattering phase shifts, $\delta_l = \frac{1}{2i}\ln S_l$), i.e.,

*Present address: School of Physics, University of Melbourne, Parkville, Victoria 3052, Australia.
†Deceased.

$$\sigma(\theta) \longleftrightarrow \{\delta_l\} \longleftrightarrow V(r) \ . \quad (1)$$

In both steps there can be ambiguities. That there are phase shift ambiguities in fitting differential cross-section data is well known. In particular, fixed energy, cross-section data are limited by scattering angle to span a finite range of momentum transfer and so there must be ambiguities in any set of S_l values obtained by fitting same. It is feasible to extract the actual scattering amplitude, $f(\theta)$, from the cross section, $|f(\theta)|^2$, but only if that cross section is known at all scattering angles and if unitarity is preserved [11]. Even then there are numerical difficulties to extract the phase variation of the scattering amplitudes. But with nuclear scattering, rarely, if ever, is a cross section measured (effectively) over all scattering angles, and in most cases there are many open nonelastic channels that can be accounted for only by invoking complex scattering potentials. Thereby unitarity is lost. Ambiguities in defining the S functions (phase shifts) are to be expected, and such is the case from our analyses of the data from 1449 MeV ^{12}C-^{208}Pb and from 1503 MeV ^{16}O-^{12}C scattering. Specifically we have found several equivalent fits to the given data sets, all of which have similar statistical significance in that each fit gave a similar (good) value of the χ^2 per degree of freedom, χ^2/F; an unexpected result perhaps given that the simple McIntyre S function involves but five parameters. The diverse behavior of the corresponding inversion potentials in the sensitive radial region shows that ambiguities, existing within an apparently narrow class of potentials, can have a decisive influence on conclusions about the physics involved.

But the iterated direct methods of fitting, which assume potential shapes with parameters varied to minimize χ^2/F, also are ambiguous. The phenomenological form of optical potentials many have used to fit heavy-ion cross-section data are quite diverse. In this context, the study presented by Kobos, Brandan, and Satchler [12] is very relevant. They analyzed the cross-section data from the scattering of 1503 MeV ^{16}O ions off of ^{12}C targets and found a family of phenomenological and semiphenomenological (folding) potentials that gave diverse (SAM-like) S functions but with comparable fits to the available data. The real part of one candidate therein has features similar to those found with some inversion studies. Likewise, Satchler [13] in a very recent article has demonstrated, from analyses of the cross section from the elastic scattering of 608 MeV ^{16}O from ^{12}C, that there are also many optical model potentials which reproduce the observed data with a goodness of fit criterion (χ^2 per datum in his case) ca. 1. Those potential forms ranged from generalized Woods-Saxon through spline radial ones and they are associated with very different, but SAM-like, S functions. In the case of 1449 MeV ^{12}C scattering from ^{208}Pb, we have found that there are at least two quite different sets of parameters defining optical potentials with a Woods-Saxon shape with which direct solution of the Schrödinger equations give excellent fits to the measured data.

It is obvious though that optical model fits to data cannot be less ambiguous than the global inversion ones. With global inversion methods, in principle, all of the possible ambiguities in going from the phase shifts (S functions) to the potentials are revealed [1,14]. In contrast, optical model potential fit procedures are such that inherent ambiguities can be easily overlooked. Imposing severe constraints on the potential shape may reduce the apparent uncertainties, but often with a considerable loss of accuracy in the fit to a fairly extensive set of data. For the cases studied the data sets are not so extensive. Hence placing strong shape constraints upon the optical model potential, i.e., by assuming a Woods-Saxon form, still allows large ambiguities while retaining fits of high quality. Thus, for the usual data at a single energy as are the two sets considered, one needs a prescription to choose which if any of the S functions from those potentials is most physical. But complicating matters is the fact that the theory for the step in which the S matrix is determined from the cross-section data when the scattering is known to require complex potentials, is still rudimentary. It is not possible to extract all of the possible ambiguities in a well-defined procedure.

Although we have concentrated our attention upon the cross sections from the elastic scattering of 1449 MeV ^{12}C ions from ^{208}Pb and of 1503 MeV ^{16}O ions from ^{12}C, we reiterate that the outcomes are of very wide application. The two specific data sets are typical of many other experimental results with various light-ion projectiles and for a wide range of energies (with energies as small as 200 MeV, Sahm *et al.* [15] found such characteristic scattering results). In particular, all such cross sections have been measured over a limited range of momentum transfer (scattering angles) and their shapes are characteristic of collisions for which the S function is SAM-like [8].

We note that a few data sets are extensive and so are "exceptional" in so far as this study is concerned. In particular the almost kinematically complete data set from the study of 350 MeV ^{16}O scattering from ^{16}O [16] has been analyzed using inverse scattering methods [5], and also by using phenomenological [17] and semimicroscopic optical model interactions [18]. Only the inversion analyses gave fits to that data set with reasonable values for the goodness of fit criterion, χ^2 per degree of freedom. But such exceptional data are not the concern herein.

Details of the inversion calculations are presented briefly next in Sec. II, the results and a discussion of them are then given in Sec. III, and concluding comments are made in Sec. IV.

II. THE SEMICLASSICAL (WKB) INVERSION METHOD

As a full discussion of the semiclassical (WKB) method for fixed energy inversion studies has been presented previously [3], only the salient points are given herein. In this approach, with r_0 being the classical turning radius and $K(\lambda, r)$ being the local momentum through the interaction region, scattering phase shift functions defined by

$$\delta(\lambda) = \lambda\frac{\pi}{2} - kr_0 + \int_{r_0}^{\infty} \left[K(\lambda, r') - k\right] dr' \ , \quad (2)$$

are used to specify the "classical" deflection function,

$$\Theta(\lambda) = 2\frac{d}{d\lambda}\delta(\lambda) \ , \tag{3}$$

from which, via an Abel integral transformation, one can find the quasipotential

$$Q(\sigma) = \frac{2E}{\pi}\int_{\sigma}^{\infty} \frac{\Theta(\lambda)}{\sqrt{\lambda^2-\sigma^2}}\, d\lambda$$
$$= \frac{4E}{\pi}\frac{1}{\sigma}\frac{d}{d\sigma}\left(\int_0^{\infty}\frac{\delta(\lambda)}{\sqrt{\lambda^2-\sigma^2}}\lambda\, d\lambda\right) \ . \tag{4}$$

For scattering associated with a unitary S function, the deflection function and quasipotential are real. However, in heavy-ion scattering the S function is generally nonunitary which makes the deflection function and quasipotential both complex quantities. The scattering potential is complex as well since it is determined from the quasipotential via the Sabatier transformation, i.e.,

$$V_{\rm WKB}(r) = E\left[1 - e^{\left(\frac{-Q(\sigma)}{E}\right)}\right] \ , \tag{5}$$

so long as the there is a 1:1 correspondence between r and σ from the transcendental equation

$$r = \frac{1}{k}\sigma e^{\left(\frac{Q(\sigma)}{2E}\right)} \ . \tag{6}$$

This relationship is valid if, for the actual potential,

$$E > V(r) + \frac{1}{2}r\frac{dV}{dr} \ , \tag{7}$$

a condition that E exceeds $E_{\rm orbit}$ (the energy at which "orbiting" occurs). The integral form of the quasipotential, Eq. (4), is solved easily if one has a rational function representation of $S(\lambda)$, namely

$$S(\lambda) = S_{\rm rat}(\lambda) = \prod_{n=1}^{N}\left(\frac{\lambda^2-\beta_n^2}{\lambda^2-\alpha_n^2}\right) \ , \tag{8}$$

as then one finds

$$Q(\sigma) = 2iE\sum_{n=1}^{N}\left[\frac{1}{\sqrt{\sigma^2-\alpha_n^2}} - \frac{1}{\sqrt{\sigma^2-\beta_n^2}}\right] \ . \tag{9}$$

However, practical applications require a background or reference S function, $S_0(\lambda)$, to be combined with a rational S function to fit data, i.e., to use

$$S_{\rm expt}(\lambda) = S_0(\lambda)S_{\rm rat}(\lambda) \ . \tag{10}$$

A convenient background S function is defined by the phase shift function

$$2\delta_0(\lambda) = \eta\ln(\lambda^2+\lambda_c^2) \ , \tag{11}$$

where λ_c is a cutoff parameter; set to the value of 3η (three times the Sommerfeld parameter) in our calculations. This reference S function, $S_0(\lambda)$, corresponds to a quasi-Coulomb potential, $V_0(r)$; so defined because it varies as r^{-1} for large radii. The main task of the inversion procedure is then to find the set of complex zero-pole pairs $\{\alpha_n, \beta_n\}$ that map $S_{\rm rat}(\lambda)$ into the rational form of Eq. (8). Once they have been determined, it is straightforward to evaluate the corresponding potential via WKB inversion as the total quasipotential is the sum of the reference and rational function parts. Thence by the Sabatier transform, a total potential can be specified and expanded in the form

$$V_{\rm expt}(r) = V_{\rm nucl}(r) + V_{\rm Coul}^{\rm FS}(r) \ , \tag{12}$$

where the Coulomb potential, $V_{\rm Coul}^{\rm FS}(r)$, often is taken to be that of charged sphere of radius R_c, namely

$$V_{\rm Coul}^{\rm FS}(r) = 2\eta/r, \quad r \geq R_c, \tag{13}$$
$$= \frac{\eta}{R_c}\left(3 - \frac{r^2}{{R_c}^2}\right), \quad r < R_c \ . \tag{14}$$

The Coulomb radius R_c is the sum of those of the colliding pair.

III. RESULTS AND DISCUSSION

The McIntyre (five-parameter) model [7] for the S function is a particularly useful one with which to analyze heavy-ion elastic scattering cross sections that have a Fresnel-like diffraction pattern shape, and we consider the specific form

$$S_{\rm expt}(\lambda) = \zeta(\lambda)\exp^{2i\delta_{\rm nucl}(\lambda)} S_{\rm Coul}^{\rm point}(\lambda) \ , \tag{15}$$

with a point Coulomb S function given by

$$S_{\rm Coul}^{\rm point} = \frac{\Gamma(\lambda+\frac{1}{2}+i\eta)}{\Gamma(\lambda+\frac{1}{2}-i\eta)} \ . \tag{16}$$

The nuclear attribute has a magnitude, $\zeta(\lambda)$, and (real) phase, $\delta_{\rm nucl}(\lambda)$, given by

$$\zeta(\lambda) = \left[1+\exp\left(\frac{l_g-l}{\Delta}\right)\right]^{-1} \tag{17}$$

and

$$\delta_{\rm nucl}(\lambda) = \mu\left[1+\exp\left(\frac{l-l_{g'}}{\Delta'}\right)\right]^{-1} \ . \tag{18}$$

Calculations of cross sections in a search to fit data use these functions at the values $\lambda = l + \frac{1}{2}$.

Light-ion collisions, such as the scattering of 1503 MeV ^{16}O ions from ^{12}C, show a pattern more typical of Fraunhofer diffraction, and their analyses may need the addition of Regge pole terms to the McIntyre S function so that with $S_M(\lambda)$ given by Eq. (15)

$$S_{\rm expt}(\lambda) = S_M(\lambda) + i\frac{D_R(\lambda)\exp(i\varphi_R)}{(\lambda-\lambda_R)+i\frac{1}{2}\Gamma_R(\lambda)} \ , \tag{19}$$

wherein, with φ being a phase parameter and λ_R the Regge centroid, the strength and width functions are defined by

TABLE I. McIntyre model S function parameter values for 1449 MeV ^{12}C-^{208}Pb scattering and McIntyre and Regge pole parameter values for 1503 MeV ^{16}O-^{12}C scattering. The numbers in square brackets denote the power of ten.

	^{12}C-^{208}Pb				^{16}O-^{12}C	
χ^2	49.98	51.99	50.52	54.96	96.10	96.18
χ^2/F	0.96	0.99	0.97	1.05	1.71	1.72
l_g	2.660866 [2]	2.540594 [2]	2.437636 [2]	2.651409 [2]	7.62100 [1]	7.68290 [1]
Δ	2.399600 [1]	2.273590 [1]	3.546050 [1]	2.090220 [1]	1.15670 [1]	1.09720 [1]
μ	1.298788 [2]	2.068230 [1]	2.688140 [1]	3.730035 [2]	1.68772 [2]	1.67974 [2]
$l_{g'}$	2.077669 [2]	2.918400 [2]	2.815130 [2]	1.701953 [2]	5.81900 [1]	5.59410 [1]
Δ'	2.019260 [1]	3.095860 [1]	3.887670 [1]	2.634440 [1]	1.26160 [1]	1.27740 [1]
D_R^0	—	—	—	—	3.89260 [3]	3.31781 [5]
Γ_R^0	—	—	—	—	7.80344 [4]	4.44840 [6]
λ_R	—	—	—	—	-2.80076 [4]	-2.39480 [7]
φ	—	—	—	—	-3.39100 [1]	3.31780 [2]

$$\begin{pmatrix} D_R(\lambda) \\ \Gamma_R(\lambda) \end{pmatrix} = \begin{pmatrix} D_R^0 \\ \Gamma_R^0 \end{pmatrix} \{1 - \mathcal{R}[S_M(\lambda)]\} \ . \qquad (20)$$

The McIntyre S function, Eq. (15), was used to fit the ^{12}C-^{208}Pb scattering data and the various sets of parameter values so found are shown in the first four columns of Table I. The remaining columns in that table give the parameter values of the McIntyre plus Regge pole S functions that were used in the analyses of the ^{16}O-^{12}C scattering data. Each column is identified by the χ^2/F value obtained from the fit made to the relevant experimental cross-section data. Clearly, using these parameter sets lead to equivalent, excellent fits to the data; and ones that are of high statistical significance.

A. The ^{12}C-^{208}Pb scattering

The four McIntyre S functions defined by the parameter values given in the first four columns of Table I all give equivalent, excellent fits to the ^{12}C-^{208}Pb elastic scattering cross-section data. But those S functions are very different as is illustrated in Fig. 1 in which their moduli and phases are displayed. Note that the phase shifts are continuous functions of λ, but are given herein in the modulus π convention to facilitate comparisons of the quite different forms. The solid line portrays the S function corresponding to the χ^2/F=0.96 fit, the long-dashed line the χ^2/F=0.99 fit, the small-dashed line the χ^2/F=0.97 fit, and the dash-dotted line the χ^2/F=1.05 fit. All the $|S|$ results display approximately the same angular momentum variation, except the χ^2/F=1.05 result which is clearly dependent on a much larger set of partial waves than the others. This should manifest in a larger sensitive radial region in the corresponding inversion potential. The nuclear phases are shown in the bottom panel of Fig. 1 and it is evident that there are significant variations. These differences are reflected in the associated inversion potentials.

For each of the McIntyre functions specified by the parameter values listed in Table I, a set of complex zero-pole pairs $\{\alpha_n, \beta_n\}$ was found in a mapping to a corresponding rational form S function. With these sets of values, $\{\alpha_n, \beta_n\}$, the associated quasipotentials $Q(\sigma)$ were calculated and, by solving the transcendental equations, Eqs. (5) and (6), the nuclear inversion potentials at the correct radial points were deduced. Such potentials we designate hereafter as the McIntyre class of inversion potentials. In all cases, direct solutions were made of the Schrödinger equations containing the inversion potentials, and the input S functions were reproduced.

The nuclear inversion potentials for ^{12}C-^{208}Pb scattering are shown in Fig. 2. The top panels show the real and imaginary potentials over the entire radial range. The

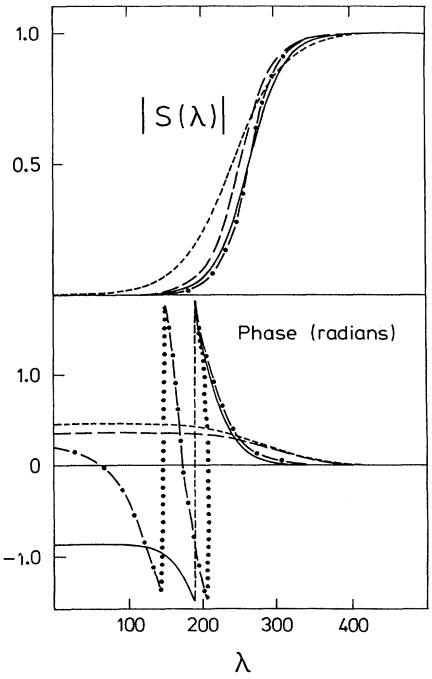

FIG. 1. The modulus (top) and phase (bottom) of the SAM (McIntyre) S functions for ^{12}C-^{208}Pb scattering. The solid line is the S function corresponding to the χ^2/F=0.96 fit, the (large) dashed line the χ^2/F=0.99 fit, the (small) dashed line the χ^2/F=0.97 fit, and the dash-dotted line the χ^2/F=1.05 fit. The phases are displayed modulo π by the dotted line connections.

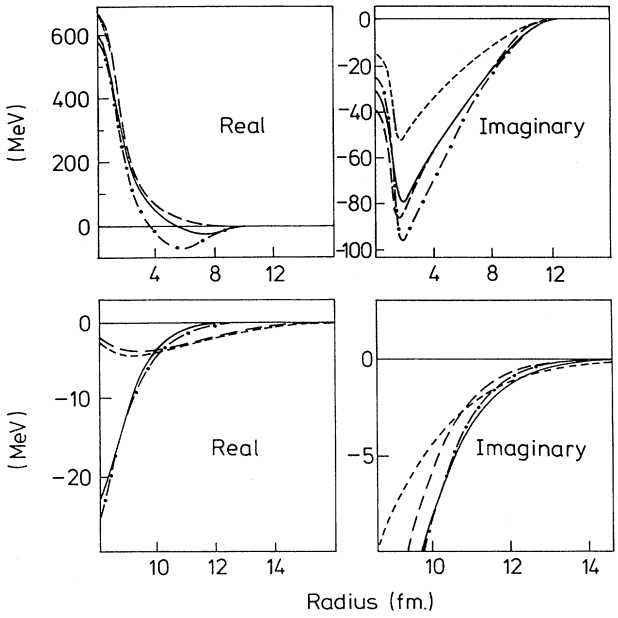

FIG. 2. The nuclear inversion potentials for ^{12}C-^{208}Pb scattering. The top panel shows the real parts of the potentials and their large radii enhancements, and the bottom panels show the same for the imaginary parts of those potentials. In both cases, the solid line is the inversion potential corresponding to the χ^2/F=0.96 fit, the (large) dashed line the χ^2/F=0.99 fit, the (small) dashed line the χ^2/F=0.97 fit, and the dash-dotted line the χ^2/F=1.05 fit.

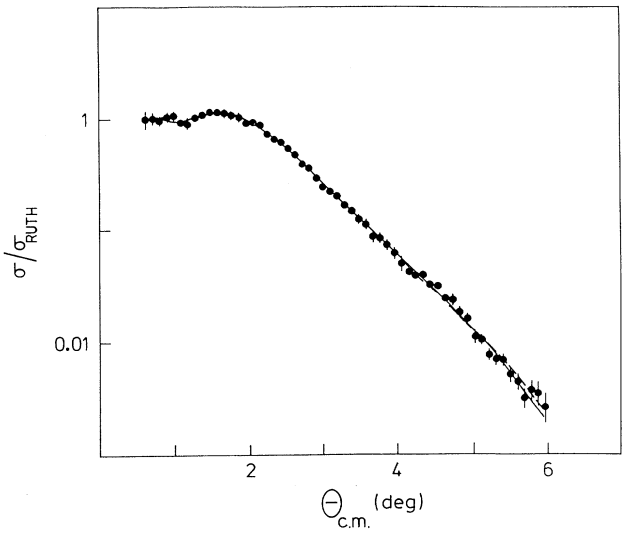

FIG. 3. The differential cross section for ^{12}C-^{208}Pb scattering. The solid line corresponds to the χ^2/F=0.96 fit, the dashed line the χ^2/F=0.99 fit. The χ^2/F=0.97 and the χ^2/F=1.05 fit results respectively are not shown herein as they lie underneath the other two.

curve identification is as given for the discussion of Fig. 1. In the bottom panel, enlarged sections of these potentials are given to emphasize their variation through the sensitive radial region (around 9.5 fm for this reaction). All of the real potentials display the short ranged repulsion that is typical of strong absorption parametrizations [4] but note that such are not in the sensitive radial region i.e., they do not affect cross-section calculations noticeably in the range of measured scattering angles. However, both the range and strength of the potentials in the sensitive radial region vary considerably. The enhancements (of the real potentials) given in the bottom section, show distinctly the significant differences of these potentials; differences that reflect in the variations of the S functions that were displayed in Fig. 1. This is less evident in the plots of the imaginary parts of the inversion potentials, but it is interesting to compare the relative strengths of the absorptive character of these potentials. In Table II, the strengths of the real potentials, $V(r)$, and the ratios of the real to imaginary potentials, $[V(r)/W(r)]$, are displayed at three radii around the so-called, strong absorption radius (approximately 9.5 fm). There is a wide variation in the real potential strengths at the selected radii and the ratios (of the real and imaginary potentials) increase with radius for the χ^2/F=0.99 and the χ^2/F=0.97 potentials but decrease for the χ^2/F=0.96 and χ^2/F=1.05 results. Clearly then, even within the McIntyre class of inversion potentials, there are ambiguities in defining the best potential to fit differential cross-section data, and to emphasise that, we show in Fig. 3 the differential cross sections for ^{12}C-^{208}Pb scattering obtained by each calculation in comparison with the data [9]. The solid line corresponds to the χ^2/F=0.96 fit, the dashed line the χ^2/F=0.99 fit. The χ^2/F=0.97 and χ^2/F=1.05 fits are not displayed as the results lie within the curves shown.

But there are ambiguities also in the optical model

TABLE II. Potential strengths, V, and ratios, V/W, at radii of 9.0, 9.5, and 10.0 fm for the scattering of 1449 MeV ^{12}C ions from ^{208}Pb.

	9.0 fm		9.5 fm		10.0 fm	
χ^2/F	V (MeV)	V/W (MeV)	V (MeV)	V/W (MeV)	V (MeV)	V/W (MeV)
0.96	-11.25	0.78	-6.49	0.59	-3.53	0.45
0.99	-3.97	0.32	-3.92	0.45	-3.75	0.66
0.97	-4.50	0.60	-4.33	0.76	-4.04	0.96
1.05	-11.66	0.72	-7.22	0.60	-4.34	0.53
1.02(opt)	-5.45	0.35	-4.21	0.37	-3.24	0.42
0.99(opt)	-7.04	0.43	-5.03	0.42	-3.60	0.45

TABLE III. Phenomenological optical model potential parameters.

		V_0	r_0	a_0	W_0	r_i	a_i	r_c
^{12}C-^{208}Pb	Set 1	286.950	0.187	1.893	24.150	1.147	0.754	1.3
	Set 2	221.986	0.492	1.451	28.970	1.124	0.790	1.3
^{16}O-^{12}C		71.434	0.924	0.767	32.959	1.004	0.724	0.86

fits to these heavy-ion collision data even with strong restrictions placed upon the potentials shapes; restrictions which may have little or no theoretical foundation. Almost from the earliest use, the "$VR^{2+\epsilon}$" ambiguity of nucleon-nucleus interactions was noted [19], and for heavy-ion collisions there has been a debate as to whether the optical potentials should be deep or shallow [20]. With the ^{12}C-^{208}Pb scattering reaction considered, we have been able to find two-parameter sets of a phenomenological optical potential of a Woods-Saxon shape,

$$V_{\rm om}(r) = V_0\left[1+\exp\left(\frac{r-r_0A^{\frac{1}{3}}}{a_0}\right)\right]^{-1} + iW_0\left[1+\exp\left(\frac{r-r_iA^{\frac{1}{3}}}{a_i}\right)\right]^{-1} + V_{\rm Coul}(r_c,r) \tag{21}$$

with which quality fits to the data were obtained. The Coulomb interaction was that between a point projectile interacting with a charged sphere of radius the sum of the two ion radii, i.e., $r_c(A_1^{1/3}+A_2^{1/3})$. The cross sections that result are indistinguishable from those presented previously in Fig. 3 and are characterized by χ^2/F values of 1.02 and 0.99 for calculations in which the parameter sets 1 and 2 were used, respectively. Those two sets of parameter values are listed in Table III and the two phenomenological potentials defined by them are compared in Fig. 4 with two of the inversion results. The inversion potentials shown therein are those with which are associated the χ^2/F fit values of 0.96 and 0.99 and are displayed by the solid and long dashed curves, respectively. The phenomenological potentials are shown by the small dashed and dotted curves for the set 1 and set 2 parametrizations, respectively. The complete radial variation of these potentials are given in the top panels of Fig. 4 from which it is clear that the two phenomenological interactions are quite different from the inversion ones. The differences between the two optical model potentials are similar in size to those between the two inversion potentials shown. Differences remain even when comparison is made through the sensitive radial region as well, as is displayed in the bottom panels of Fig. 4. In the sensitive radial region, the real parts of the phenomenological potentials lie halfway between the real parts of the two inversion results. Specific values and ratios of the optical model potentials at select radii are listed in the bottom section of Table II.

The S functions associated with the two phenomenological optical model potentials are compared in Fig. 5

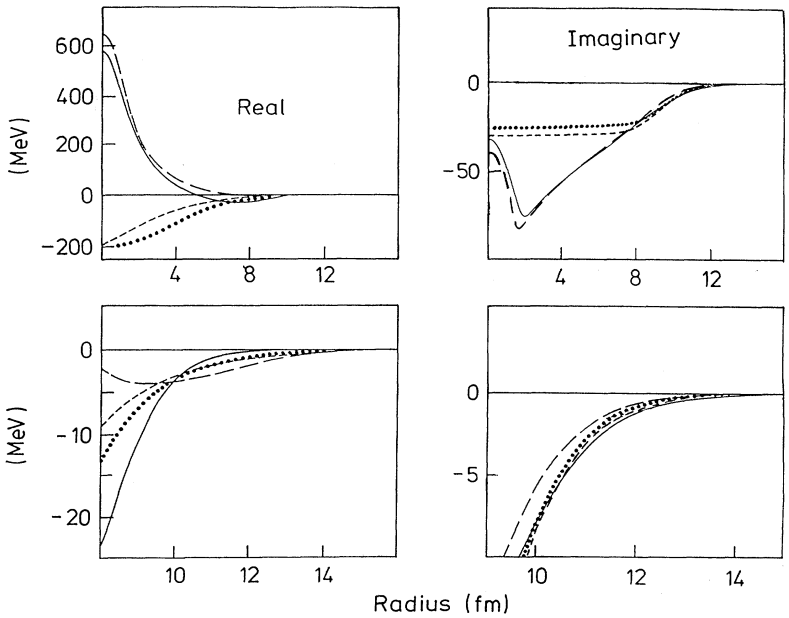

FIG. 4. Phenomenological optical model potentials for ^{12}C-^{208}Pb scattering shown by the small-dashed and dotted curves compared with the inversion potentials for which χ^2/F are 0.96 (solid curves) and 0.99 (long-dashed curves).

with those of the two McIntyre functions used to find the inversion potentials with which those optical potentials were compared in Fig. 4. Only the most important angular momentum range is displayed. The moduli are compared in the top segment and the phases, in radians, in the bottom segment. The optical model results are shown by the dash-dotted and dotted curves for the set 1 and set 2 cases while the 0.96 and 0.99 McIntyre fit functions are displayed by the solid and dashed curves, respectively.

Finally, in Fig. 6, the differential cross sections evaluated using each of the S functions we have considered, are shown for scattering angles to 20°; a range far beyond that of the available data. In the top panel of Fig. 6, the cross sections found using the four McIntyre S functions are compared with the data (displayed therein by the large dots). The notation is as used in Fig. 1 save that the results found with the $\chi^2/F = 0.97$ case are displayed now by the dotted curve. In the bottom panel, the two optical model and two McIntyre results are shown with the notation being that used in the discussion of Fig. 5. From these diagrams it is evident that the ambiguity in all of the potentials is due mainly to the limited nature of the available data set. Although calculated results found using each of the inversion potentials fit the measured data equally well, they differ dramatically at larger scattering angles. Clearly measured data to larger scattering angles would differentiate between the set of four potentials if one of them should fit such an extended data set. It is interesting to note that it would require measurements accurate up to 5 orders of magnitude (out to 8°) to distinguish between the potential associated with the cross section portrayed by the dotted curve in the top panel of Fig. 6 and the other three inversion potentials,

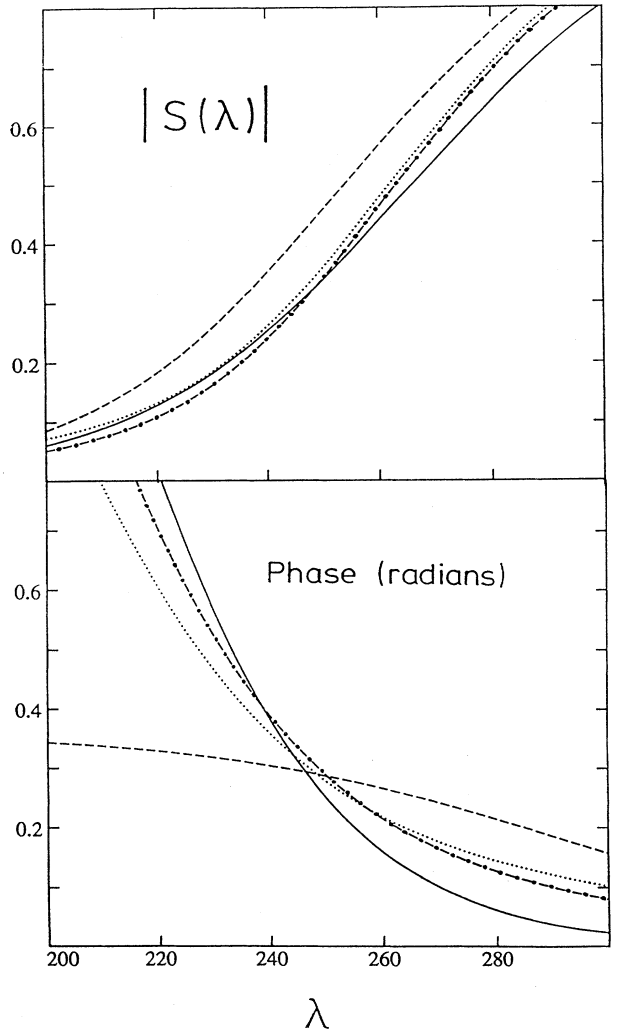

FIG. 5. The S functions, moduli (top) and phases (bottom), associated with the two optical models and the two inversion potentials that were compared in Fig. 4. The results for the set 1 and set 2 optical model potentials are displayed by the dash-dotted and dotted curves, respectively. The solid and dashed lines portray the inversion functions for the χ^2/F cases of 0.96 and 0.97, respectively.

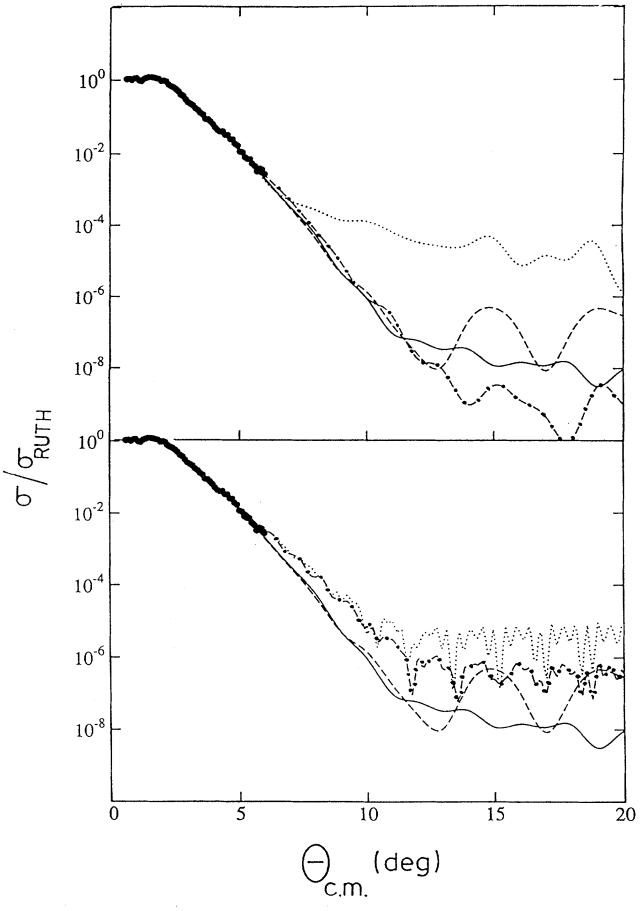

FIG. 6. Differential cross sections for 1449 MeV ^{12}C-^{208}Pb scattering shown to 20° scattering angle. The top panel compares the four cross sections calculated by using the four McIntyre S functions from which the McIntyre class of inversion potentials were obtained. The bottom panel shows the phenomenological optical model potential results compared with those of the two inversion cases for which the potentials and S functions were shown in Figs. 4 and 5, respectively.

which might just be feasible given recent experimental results from heavy-ion scattering [16]. However if the three other potentials would correctly predict such new data (a variation in the cross section over seven orders), an extremely (unlikely) precise experiment would be required to clearly distinguish between them. Of course it is possible that data measured down to 8°, would eliminate all four potentials. However even in that case, it is still probable that we could produce another set of potentials from fits to that extended range data set, but different beyond and in such a manner that only measurements requiring highly unrealistic variation of the cross section of 7–10 orders of magnitude would be able to eliminate some or all of them. Additional physical input would be required to discriminate between such potentials. Similar statements are true in large measure when one compares the phenomenological optical model potential results with those of the (two) inversions as is done in the bottom segment of the figure.

B. The ^{16}O-^{12}C scattering

The measured ratio to Rutherford cross sections from the 1503 MeV ^{16}O-^{12}C elastic scattering [10] are given in Fig. 7. Those data are compared therein with the results of our inversion calculations. The solid and long-dashed curves depict the results obtained by using two inversion potentials from the S functions for which the fits to the data are classified by χ^2/F values of 1.71 and 1.72, respectively. The optical model fit underlies these two results, although with it the χ^2/F value is 3.0. It is more difficult to fit the typical Fraunhofer diffraction shape of this data than the Fresnel-like shape of the ^{12}C-^{208}Pb data and that is reflected by the larger χ^2/F values. The scattering of light ions is not as strongly absorptive although the S functions that give the fits do have SAM-like shape. That is shown in Fig. 8 wherein the three S functions, two inversion and the single optical model cases, are displayed. The two inversion functions are given by the solid and dashed curves again, while the optical model function is shown by the dotted curves now. The SAM-like form of the magnitudes of these S functions is evident, but the small λ values are not vanishingly small now. Also the two inversion results are not extremely different, but the optical model result is dissimilar to both the others. The parameter values that led to these three results are given in Table I for the two inversion studies and in Table III for the optical model. The McIntyre S functions in these cases had to supplemented by a single Regge pole term to get fits of 1.71 and 1.72 for the χ^2/F, respectively.

Both McIntyre plus Regge pole S function forms were mapped onto a four-term rational function form to effect WKB inversion calculations of the potentials. In this case the sensitive radial region (for the data used) extends from $\sim$ 2 fm outwards. In that region the two inversion potentials are not very different as is evident from Fig. 9 wherein they are compared with the "best fit" standard optical model potential. The differences between the two inversion potentials and the optical model are appreciable however. It is true that the optical model interaction does not fit the data as well (χ^2/F was 3.0 compared with 1.71 and 1.72) but it is good enough for our pur-

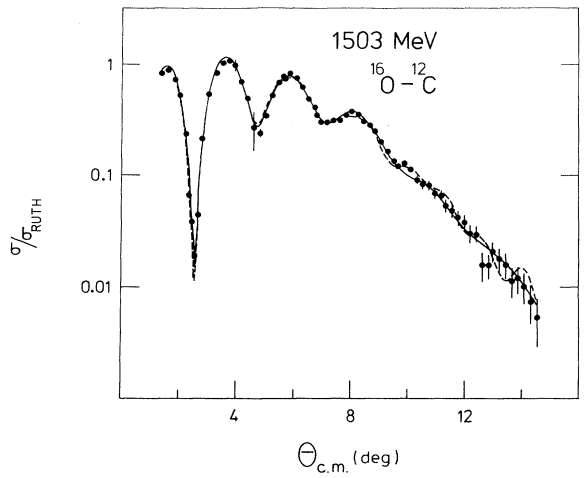

FIG. 7. Differential cross-section data for 1503 MeV ^{16}O-^{12}C scattering shown as ratio to Rutherford and compared with the results of two inversion calculations and a single optical model potential calculation. The inversion potentials led to the cross sections shown by the solid and long-dashed curves for the cases of χ^2/F being 1.71 and 1.72, respectively. The optical model calculation resulted in a cross section indistinguishable (on this scale) from the two shown.

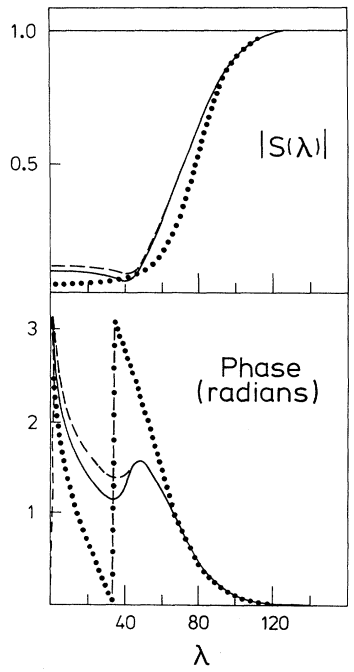

FIG. 8. The S functions for the two inversion cross sections given in Fig. 7, and for that of the optical model calculation (displayed by the dotted curves). The magnitudes are shown in the top section and the phases are given (modulo π depicted by the dot-dashed connection) in the bottom part.

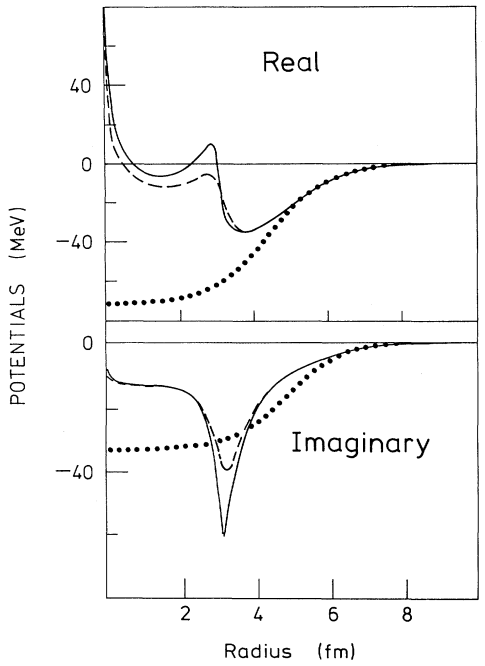

FIG. 9. The inversion and optical model potentials from the analyses of the 1503 MeV ^{16}O-^{12}C data. The inversion potentials are shown (again) by the solid and dashed curves while those of the optical model are shown by the dotted curves.

pose especially as the Kobos-Brandan-Satchler [12] study demonstrated that comparably good fits to this same data can be found with diverse Woods-Saxon potentials; some having quite strong absorption. That is also the case at lower energy as Satchler [13] has shown with his extensive optical model analyses of the cross-section data from the elastic scattering of 608 MeV ^{16}O ions from ^{12}C. He found numerous local optical model potentials of generalized Woods-Saxon, semimicroscopic and spline radial forms that led to equivalent, very good fits to the data; epitomized by values of the χ^2 per datum of order 1. He concluded that a single energy experimental cross section would not, in general, be sufficient to establish the validity of any model interaction for the colliding ions. Our results confirm that.

It is also of note that a pure McIntyre S function (no Regge pole addition) can be found that fits the data with a value of $\chi^2/F \sim 5$. This is a strong absorption result similar to the strong absorption optical model potentials of the set of Kobos, Brandan, and Satchler [12]. Thus with analyses of typical Fraunhofer-like data, the difference between fit values (χ^2/F) of 5 and ca. 1 may be of some significance. Nevertheless, even with a better fit criteria, our results indicate that one may still expect residual ambiguities in the analysis of that typical data.

IV. CONCLUSIONS

Fixed energy inverse scattering methods have been applied to extract inversion potentials from measured differential cross sections from 1449 MeV ^{12}C-^{208}Pb and from 1503 MeV ^{16}O-^{12}C collisions. Those data sets are typical of many measured results having Fresnel and Fraunhofer diffractionlike shapes, respectively, and with data measured over a quite limited range of momentum transfer values. The data also can be fit with S functions characteristic of strong absorption models of scattering.

A semiclassical (WKB) inversion scheme was used to ascertain complex, local interactions but the first step in the procedure was to fit the differential cross-section data with a McIntyre form for the S function, supplemented by a Regge pole term in the case of the ^{16}O-^{12}C scattering. Several excellent fits to the ^{12}C-^{208}Pb data were found with $\chi^2/F \approx 1$ while good ones ($\chi^2/F \approx 1.7$) were obtained from the ^{16}O-^{12}C analyses. Each McIntyre or McIntyre plus Regge pole S function then was mapped into a rational function form with which the inversion was performed. The derived inversion potentials are smooth, well-behaved functions. But in the sensitive radial region and for both the ^{12}C-^{208}Pb and ^{16}O-^{12}C cases, there are marked differences in the strengths of the respective real and imaginary potentials. Also the details of the shapes of these potentials are rather different and, given the equivalent fits to data with which each is associated, such variation is a measure of ambiguities in defining the nuclear part of heavy-ion optical potentials based solely upon most currently available data. There were little if no disparities between the inversion potentials we found from a fit to the ^{16}O-^{12}C data at least through the sensitive radial region, but optical model fits of similar quality gave results that are quite different. The structured Fraunhofer-like shapes of light-ion collisions are more restrictive then in what ambiguity one has in fitting the data and with what potentials give those fits. But ambiguities exist nevertheless.

The ambiguities associated with Fresnel-like input can be associated with large relative differences in the cross section beyond the angular range of measurements. But to discriminate between the ^{12}C-^{208}Pb potentials would require accurate measurements over 7–10 orders of magnitude in the cross section, which is beyond reasonable expectations. Whatever improved extended data set could be found, and even if that eliminated all of the potentials specified herein, we believe that ambiguities in the analysis will remain. What is particularly serious are the marked differences even in the sensitive radial region of the (Fresnel) potentials, which severely diminishes the hope that an increased angular range of measurements corresponds to an improved determination of the potential at shorter distances only, i.e., without affecting knowledge of the longer range attributes. This is a consequence not of the WKB inversion from $\{\delta_l\}$ to $V(r)$ but is due to the ambiguities in the step from $\sigma(\theta)$ to $\{\delta_l\}$.

We conclude that these results obtained by means of inverse scattering methods highlight that making more extensive and detailed measurements of cross-section data will not necessarily provide a deeper understanding of heavy-ion collisions, especially as even potential fitting with very prescribed potential shapes has also been shown to be ambiguous. Additional physical input to the

study will be needed. Good semimicroscopic model fits to typical data sets do not suffice. Our study has shown that such data do not constrain the S function enough. If theoretical model calculations (based upon credible underlying two nucleon g matrices and nuclear structure functions) are sought to alleviate the ambiguity problems we have ellucidated, they must produce high accuracy fits to data sets that are more extensive than usually available, i.e., give fits of statistical significance to data such as that from the 350 MeV elastic scattering of ^{16}O ions from ^{16}O as measured recently [16]. The poor quality fits to some of the exceptional data so far obtained with "realistic" microscopic model optical model calculations [18] (even with those that are semiphenomenological having parameterized forms for the imaginary potential) do not provide a statistically meaningful confirmation of such a theory. But, if the theoretical model fits could be made with sufficient accuracy, then they can be used to regularize potentials obtained via a highly accurate inversion. Such a regularized inversion process would reduce the scope of the ambiguities as to what is the "physical" S function and therefore of the interaction whether the analysis is direct or inverse. But to do so, not only the data but also the theoretical models must be improved considerably in the future if further progress is to be made.

[1] K. Chadan and P. S. Sabatier, *Inverse Problems in Quantum Scattering Theory*, 2nd ed. (Springer, Berlin, 1989).

[2] R. Lipperheide, H. Fiedeldey, and H. Leeb, in *Advanced Methods in the Analysis of Nuclear Scattering Data*, Lecture Notes in Physics Vol. 236, edited by H. C. Krappe and R. Lipperheide (Springer, Berlin, 1985), and references cited therein; H. Leeb, H. Fiedeldey, and R. Lipperheide, Phys. Rev. C **32**, 1223 (1985); S. G. Cooper, M. W. Kermode, and L. J. Allen, J. Phys. G **12**, L291 (1986); R. S. Mackintosh and S. G. Cooper, Nucl. Phys. **A494**, 123 (1989).

[3] E. J. Kujawski, Phys. Rev. C **6**, 709 (1972); **8**, 100 (1973); H. Fiedeldey, R. Lipperheide, K. Naidoo, and S. A. Sofianos, *ibid.* **30**, 434 (1984); K. Naidoo, H. Fiedeldey, S. A. Sofianos, and R. Lipperheide, Nucl. Phys. **A419**, 13 (1984); L. J. Allen, K. Amos, C. Steward, and H. Fiedeldey. Phys. Rev. C **41**, 2021 (1990); L. J. Allen, H. Fiedeldey, S. A. Sofianos, K. Amos, and C. Steward. *ibid.* **44**, 1606 (1991); L. J. Allen, K. Amos, and H. Fiedeldey, J. Phys. G **18**, L179 (1992).

[4] H. Leeb, C. Steward, K. A. Amos, and L. J. Allen, Phys. Rev. C **45**, 2919 (1992).

[5] L. J. Allen, L. Berge, C. Steward, K. Amos, H. Fiedeldey, H. Leeb, R. Lipperheide, and P. Fröbrich, Phys. Lett. B **298**, 36 (1992).

[6] W. E. Frahn, in *Treatise on Heavy Ion Science*, edited by D. A. Bromley (Plenum, New York, 1984), Vol. 1, and references cited therein.

[7] J. A. McIntyre, K. H. Wang, and L. C. Becker, Phys. Rev. **117**, 1337 (1960).

[8] M. C. Mermaz, Z. Phys. A **321**, 613 (1985); M. H. Cha and Y. J. Kim, J. Phys. G **16**, L281 (1990).

[9] J. Y. Hostachy, M. Buenerd, J. Chavin, D. Lebrun, Ph. Martin, J. C. Lugol, L. Papineau, P. Roussel, N. Alamanos, J. Arvieux, and C. Cerruti, Nucl. Phys. **A490**, 441 (1988).

[10] P. Roussel-Chomaz, N. Alamanos, F. Auger, J. Barrette, B. Berthier, B. Fernandez, L. Papineau, H. Coubre, and W. Mittig, Nucl. Phys. **A477**, 345 (1988).

[11] R. B. Gerber and M. Karplus, Phys. Rev. D **4**, 998 (1970); R. B. Gerber, M. Shapiro, U. Buck, and J. Schleusener, Phys. Rev. Lett. **41**, 236 (1978).

[12] A. M. Kobos, M. E. Brandan, and G. R. Satchler, Nucl. Phys. **A487**, 457 (1988).

[13] G. R. Satchler, Nucl. Phys. **A574**, 575 (1994).

[14] M. Cuer, Ann. Phys. (N.Y.) **120**, 1 (1979).

[15] C.-C. Sahm, T. Murakami, J. G. Cramer, A. J. Lazzarini, D. D. Leach, D. R. Tieger, R. A. Loveman, W. G. Lynch, M. B. Tsang, and J. van der Plicht, Phys. Rev. C **34**, 2165 (1986).

[16] E. Stilliaris, H. G. Bohlen, P. Fröbrich, B. Gebauer, D. Kolbert, W. von Oertzen, M. Wilpert, and Th. Wilpert, Phys. Lett. B **233**, 291 (1989).

[17] M. E. Brandan, K. W. McVoy, and G. R. Satchler, Phys. Lett. B **281**, 185 (1992).

[18] D. T. Khoa, W. von Oertzen, A. Faessler, M. Ermer, and H. Clement, Phys. Lett. B **260**, 278 (1991).

[19] P. E. Hodgson, *The Optical Model of Elastic Scattering* (Clarendon Press, New York, 1962).

[20] K. Aoki and H. Horiuchi, Prog. Theor. Phys. **69**, 1154 (1983).